



Ultrasonic-assisted synthesis of Fe₃O₄ nanoparticles-loaded sawdust carbon for malachite green removal from aquatic solutions

Ziaeddin Bonyadi¹ · Fatemeh Sadat Khatibi¹ · Fatemeh Alipour¹

Received: 24 February 2022 / Accepted: 18 July 2022 / Published online: 9 August 2022
© The Author(s) 2022

Abstract

MG, an organic compound composed of triphenyl methane, is often widely used in various industries, especially in the food, pharmaceutical and textile industries. This study emphasizes the green synthesis of novel magnetic iron oxide nanoparticles-loaded sawdust carbon (Fe₃O₄/SC) and their effect on the removal of MG from the aqueous solution. To obtain the optimum conditions of MG removal using the Box–Behnken model, the independent variables such as the initial MG concentration (10–100 mg/L), pH (3–9), reaction time (10–60 min), and Fe₃O₄/SC nanocomposites dose (0.2–1 g/L) were experimented. According to the quadratic model, the highest removal rate (89.22%) was found at the pH of 8.62, the contact time of 59.86 min, the Fe₃O₄/SC ncs dose of 0.59 g /L and the MG level of 17.62 mg/L. The MG removal rate follows the pseudo-second-order model and the Langmuir model. The maximum absorption capacity for MG was 41.66 mg/g. These findings suggest that the Fe₃O₄/SC ncs has a significant potential for the MG adsorption from aqueous solution.

Keywords Fe₃O₄/SC · Malachite green · Kinetics · Isotherms · Adsorption

Abbreviations

| | |
|------------------------------------|---|
| MG | Malachite green |
| Fe ₃ O ₄ /SC | Magnetic iron oxide nanoparticles-loaded sawdust carbon |
| Ncs | Nanocomposites |
| FT-IR | Fourier-transform infrared spectroscopy |
| pHzpc | Zero point of charge |
| EDX | Energy-dispersive X-ray |
| FESEM | Field emission scanning electron microscopy |
| DLS | Dynamic light scattering |
| ANOVA | Analysis of variance |
| BBD | Box–Behnken design |

Introduction

Dyes are common pollutants released from various industries, especially the textile industry. In the early nineteenth century, dyes often originated naturally from animals and plants. After this period, the industrial production of dye was

performed in 1977 and gradually synthetic dyes replaced natural type (Selvaraj et al. 2021). The annual production of about 10,000 types of synthetic dyes has caused a large amount of this pollutant to enter the environment (Chowdhury et al. 2020). Azo dyes are considered as a serious threat for human health and the environment due to their toxic nature (Chowdhury et al. 2020). These pollutants are difficultly removed from aqueous solutions due to their aromatic hydrocarbon functional groups and the complexity of their molecular structure (Ramavandi et al. 2019). Azo dyes are chemical class of dyes, which are characterized by the presence of at least one azo bond (–N==N–) bearing aromatic rings, and dominate the worldwide market of dyestuffs with a share of about 70% (Ramavandi et al. 2014).

Malachite green, an organic compound composed of triphenyl methane, is often widely used in various industries, especially in the food, pharmaceutical and textile industries (Fan et al. 2021). This dye is also used to treat microbial infections of fish. However, this toxic contaminant remains in the water for a long time due to its slow biodegradability by microorganisms (Qu et al. 2019). The discharge of high concentrations of MG into aquatic ecosystems prevents the natural light penetration into the water, which leads to a decrease in oxygen content and inhibition of aquatic activity due to reduced photosynthetic efficiency of plants (Wang et al. 2017). This reactive dye has carcinogenic, mutagenic and teratogenic properties in

✉ Ziaeddin Bonyadi
Bonyadiz@mums.ac.ir

¹ Department of Environmental Health Engineering, School of Health, Mashhad University of Medical Sciences, Mashhad, Iran

human. Furthermore, MG causes the health problems such as chromosomal abnormalities and gastrointestinal irritation for human (Tkaczyk et al. 2020). Therefore, it is necessary to use effective techniques for the removal of MG from dye wastewater. For this purpose, various methods have been considered to remove this pollutant from the environment. Among these, the treatment of dye wastewater using the adsorption method is very attractive due to its advantages such as simplicity, low cost and high efficiency (Saini et al. 2017). Bonyadi et al. (2022) removed successfully malachite greens from aquatic environments using *Spirulina platensis* (Bonyadi et al. 2022).

Nanotechnology is a relatively new branch of science that has wide applications in the field of treatment and control of environmental pollutants. The use of nanoparticles due to its high adsorption capacity, large surface area and high reactivity is a common strategy for the treatment of dye effluents and an effective alternative for conventional treatment methods (Joshi et al. 2018). Recently, new nanostructures have been used to purify azo dyes. The performance of nanoparticles depends mainly on the dye structure, the type of nanoparticles used and the related functional groups (Joshi et al. 2019). Magnetic nanoparticles are usually used for the removal of dyes from wastewater flow, even at very low concentrations (Joshi et al. 2019). Among the various types of magnetic nanoparticles, the use of iron nanoparticles has attracted much attention due to its low cost, easy synthesis, high catalytic activity and high potential reactivity (Liu et al. 2016). The green synthesis of magnetic nanoparticles is an appropriate economic and environmental approach. In this approach, natural biopolymers can be used due to low cost, high availability, strong affinity for metals, biodegradability, green solvent and reducing agents. The green synthesis of nanoparticles can be carried out using biological wastes, including rice husk, pine, wood, sawdust, orange peel, plant leaves, etc. Esvandi et al. (2020) and Foroutan et al. (2021) conducted similar studies on the removal of azo dyes using magnetic nanocomposites.

Among these, saw dust is easily available, low cost, lignocellulose and has previously been utilized for the reduction of Fe^{3+} to Fe^{2+} ion (Yu et al. 2013; Bayat et al. 2015). Phenols and lignocelluloses in sawdust cause pollutant reduction (Chen et al. 2014). This paper focuses on the removal of MG from the aqueous medium by $\text{Fe}_3\text{O}_4/\text{SC}$ nanocomposite. The removal process of MG was also examined to better understand the adsorption mechanism by isotherm and kinetic studies.

Materials and methods

Chemicals and reagents

Malachite green, ferric nitrate [$\text{Fe}(\text{NO}_3)_3 \cdot 9\text{H}_2\text{O}$], and liquor ammonia (25%) were purchased from Sigma-Aldrich

Company. Sodium hydroxide pellets, hydrochloric acid, and nitric acid were bought from the Merck Company. Poplar tree sawdust was prepared from a saw mill located at Mashhad, Iran. Double-distilled water was utilized to prepare solutions in tests. The synthetic solutions at different levels were prepared from a stock MG solution of 200 mg/L.

Synthesis of $\text{Fe}_3\text{O}_4/\text{SC}$ ncs

Based on the biogenic green synthesis approach, $\text{Fe}_3\text{O}_4/\text{SC}$ ncs were provided. At the beginning, for the preparation of sawdust, it was washed several times with distilled water and dried at 60°C for 24 h. The prepared powder was passed through 100 mesh. 4.0 g of $\text{Fe}(\text{NO}_3)_3 \cdot 9\text{H}_2\text{O}$ and 3 g of sawdust powder were dissolved in 100 ml of double-distilled water, and then the resulting suspension was stirred vigorously at 90°C for 1 h. In the reaction mixture, Fe^{3+} ions are reduced to Fe^{2+} ions using a sawdust solution (green solvent). The solution was then transferred to an ultrasonic device, and during the sonication process, the pH of the solution was increased to 10 by the gradual addition of ammonia (25%). Then, the black iron oxide nanoparticles were separated from the aqueous solution using ultrasound after changing the dye of the reaction mixture from brown to black using ultrasound. $\text{Fe}_3\text{O}_4/\text{SC}$ ncs were dried at 180°C for 12 h in an electric oven (Kataria and Garg 2018). The resulting nanocomposites were stored in supportive plastic containers and used for further synthesis.

The characteristics of $\text{Fe}_3\text{O}_4/\text{SC}$ ncs

The characterization of $\text{Fe}_3\text{O}_4/\text{SC}$ nanocomposite was studied using different techniques including FT-IR (Broker victor 22), EDX (Costech ECS 4010), and FESEM (LMU TESCAN BRNO-Mira3), DLS (Horiba- SZ-100-Z).

pHzpc determination

For the determination of pHzpc, 100 mL of 0.01 M NaCl solution was poured in flasks and the pH of solutions was adjusted to around 2, 4, 6, 8, 10, and 11. Then, a 2.5 g/L of $\text{Fe}_3\text{O}_4/\text{SC}$ nanocomposite was added into the solutions, mixed at the fixed speed of 250 rpm for 24 h, and filtrated by Whatman paper 42. Finally, the difference between the initial and final pH values or " $\Delta\text{pH} = \text{pHi} - \text{pHf}$ " was plotted versus pHi.

Experimental design

In the study, a 100 mL of dye solution was prepared at the MG concentrations of 10, 55 and 100 mg/L, and under the independent variables, including $\text{Fe}_3\text{O}_4/\text{SC}$ ncs dose (0.2–1 g/L), pH (3–9), and retention time (10–60 min)

(Table 1). The dye removal process was performed on a magnetic stirrer at a speed of 250 rpm. At the end of the reaction time, the supernatant was separated from the settling portion using a centrifuge (model CE-118) at 3000 rpm for 12 min. After the adsorption occurred, the solutions centrifuged and the remaining MG dye was measured in the supernatant by the spectrophotometric method at λ_{max} of 618 nm.

The MG removal rate was obtained from the following equation:

$$\text{Removal efficiency \%} = \frac{(C_0 - C_e) \times 100}{C_0} \quad (1)$$

where C_0 is the initial MG concentration (mg/l) and C_e is the MG concentration in the treated solution after a given time (mg/L).

$$q_e = \frac{(C_0 - C_e)}{m} \times V \quad (2)$$

where W is the mass of nanocomposite adsorbent (gr) and V is the volume of reaction solution (L).

Modeling MG removal

The current study was designed using the specialized response level software (RSM), Box–Behnken model (BBD), to optimize the MG removal rate by nanocomposite. The quadratic model, used by RSM, is expressed as the following equation:

$$Y = \beta_0 + \sum_{i=1}^k \beta_i x_i + \sum_{i=1}^k \beta_{ii} x_i^2 + \sum_{1 \leq i < j} \beta_{ij} x_i x_j \quad (3)$$

where Y , β_0 , β_i , β_{ii} , β_{ij} and x_i or x_j describe the predicted response, the constant coefficient, regression coefficients for linear impacts, quadratic coefficients, interaction coefficients, and the coded values of the factors, respectively.

Table 1 Range and levels of main parameters used for the MG adsorption

| Factor | Parameter level | | | |
|---|-----------------|-----|-----|-----|
| | Code | -1 | 0 | +1 |
| Time (min) | A | 10 | 35 | 60 |
| MG concentration (mg/L) | B | 10 | 55 | 100 |
| pH | C | 3 | 6 | 9 |
| Fe ₃ O ₄ /SC dose (g/L) | D | 0.2 | 0.6 | 1 |

Adsorption kinetic and isotherm studies

Kinetic studies also composed an essential section of the sorption check that reveals significant information for real treatment system design. The study of adsorption kinetics was investigated using independent variables, including the initial MG concentration (25–120 mg/L), the pH of 6, and the dose of 0.6 g/L. The adsorption kinetics of MG onto the nanocomposite were evaluated by the well-known models pseudo-first-order, pseudo-second-order, and intraparticle diffusion. Adsorption isotherms, including Freundlich, Langmuir, and Temkin isotherms, were examined in the presence of the above-mentioned variables. The equations related to kinetic and isotherm models were presented in the studies of Mohebbad et al. (2019) and Davodi et al. (2019) (Fig. 1).

Results and discussion

Characterization

FT-IR: The FT-IR spectrum for Fe₃O₄/SC ncs before and after the MG adsorption is shown in Fig. 2. In Fe₃O₄/SC ncs, the stretching vibration of F–O group at 631, 587 and 435 cm⁻¹ showed the incorporated iron oxide nanoparticles in sawdust carbon (Cheng et al. 2012). The absorption peaks

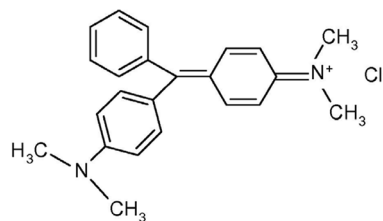


Fig. 1 Structural formula of MG

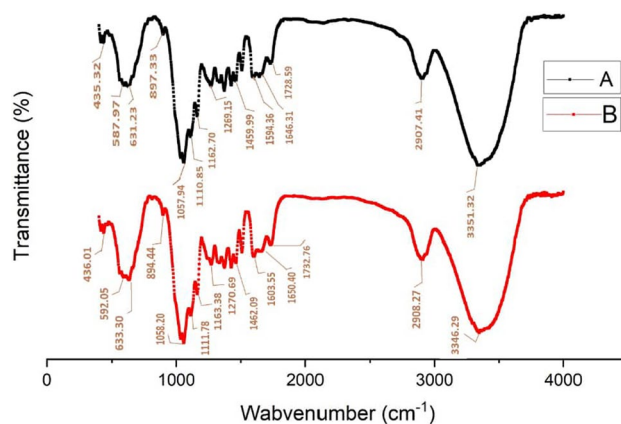


Fig. 2 FTIR spectra of (A) before and (B) after MG adsorption

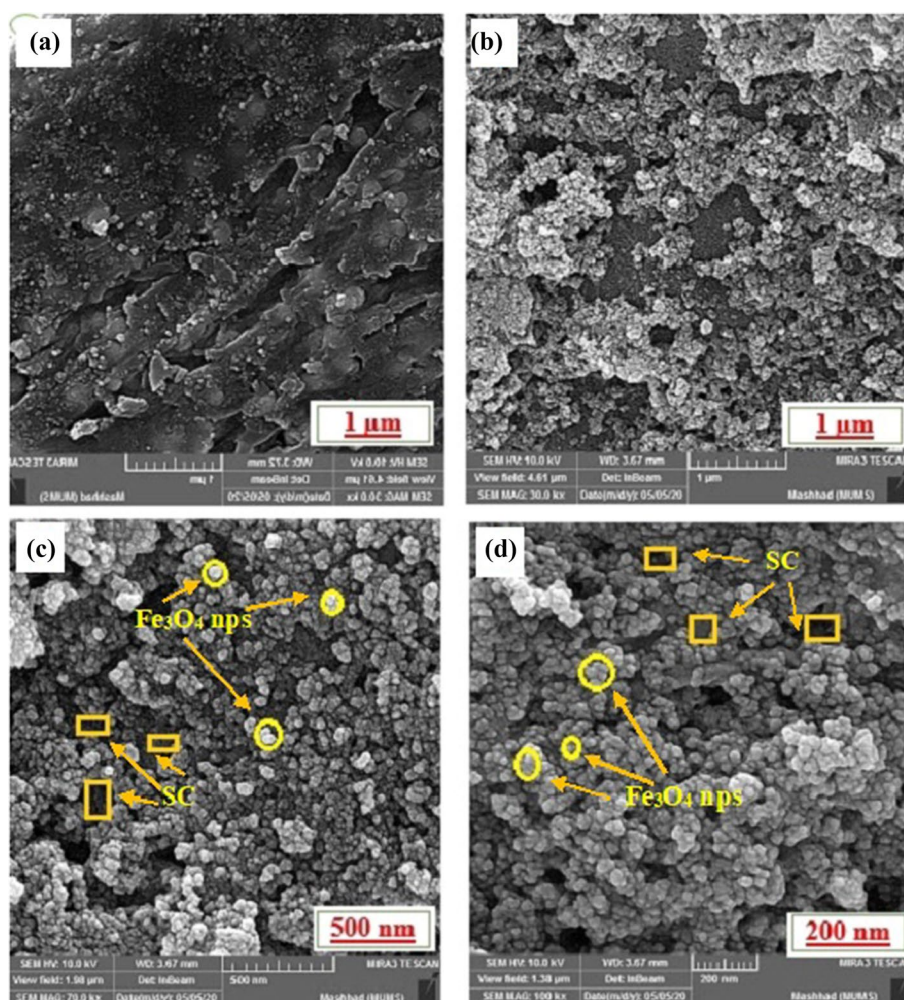
in the range of $1459\text{--}1269\text{ cm}^{-1}$ were related probably to C–H stretching vibration of methyl and methoxy groups. The peaks at 1728 , 1646 , and 1598 cm^{-1} were related to C=O stretching vibrations due to the attendance of lignin and hemicelluloses. The peaks at 2907 cm^{-1} were correlated with C–H stretching vibration of methyl and methylene group existent in magnetic sawdust carbon (Gan et al. 2016). The absorption peaks at 3351 and 3858 cm^{-1} correspond to O–H stretching vibration of lignocelluloses and water molecules. With regard to the findings, the range of vibrations and the intensity of absorption peaks in the structure of $\text{Fe}_3\text{O}_4/\text{SC ncs}$ after the MG sorption were altered, which could be due to the interaction between the functional groups and the MG. For example, after MG sorption, the some peaks related to the functional groups of F–O, C–H, C=O, and O–H were altered to 592 , 1462 , 1650 , and 3346 cm^{-1} , respectively (Gan et al. 2016). Therefore, these changes were indicating the effective attribution of these functional groups in the adsorption of MG.

FESEM: FESEM images of $\text{Fe}_3\text{O}_4/\text{SC ncs}$ are provided in Fig. 3a–d. The FESEM image shows small pieces of

sawdust fiber sheet with a mostly uneven surface (Fig. 3a). As can be seen from the FESEM images, Fe_3O_4 nanoparticles have been compounded onto the SC surface in agglomerated form as well as elsewhere. FESEM image of $\text{Fe}_3\text{O}_4/\text{SC ncs}$ shows that Fe_3O_4 nanoparticles incorporate onto the surface of sawdust carbon in agglomerated form and other places also (Fig. 3b and c). The Fe_3O_4 nps are spherical in form and prepared by SC powder as reducing factor.

EDX, DLS, and pH_{zpc} : Figure 4 indicates EDX spectra and elemental composition of SC (a), $\text{Fe}_3\text{O}_4/\text{SC ncs}$ (b), DLS spectrum of synthesized $\text{Fe}_3\text{O}_4/\text{SC ncs}$ (c), and plot between final pH versus pH_i of nanocomposites (d). According to EDX images (Fig. 4a,b), the values of C, O, N, S, and Fe in the SC were found 51.63 , 40.13 , 5.57 , 2.43 , and 0.24% , respectively. After magnetization of $\text{Fe}_3\text{O}_4/\text{SC ncs}$, the percentage of elements in the SC altered, which could be due to the reaction of the SC content with Fe_3O_4 . Due to the increase in the Fe value up to 4.49 , it can be stated that iron oxide nanoparticles are well incorporated on the sawdust carbon surface. The hydrodynamic diameter of $\text{Fe}_3\text{O}_4/\text{SC ncs}$ was measured using by DLS analysis. The Z-average

Fig. 3 FESEM images of (a) raw sawdust and (b, c, d) $\text{Fe}_3\text{O}_4/\text{SC ncs}$



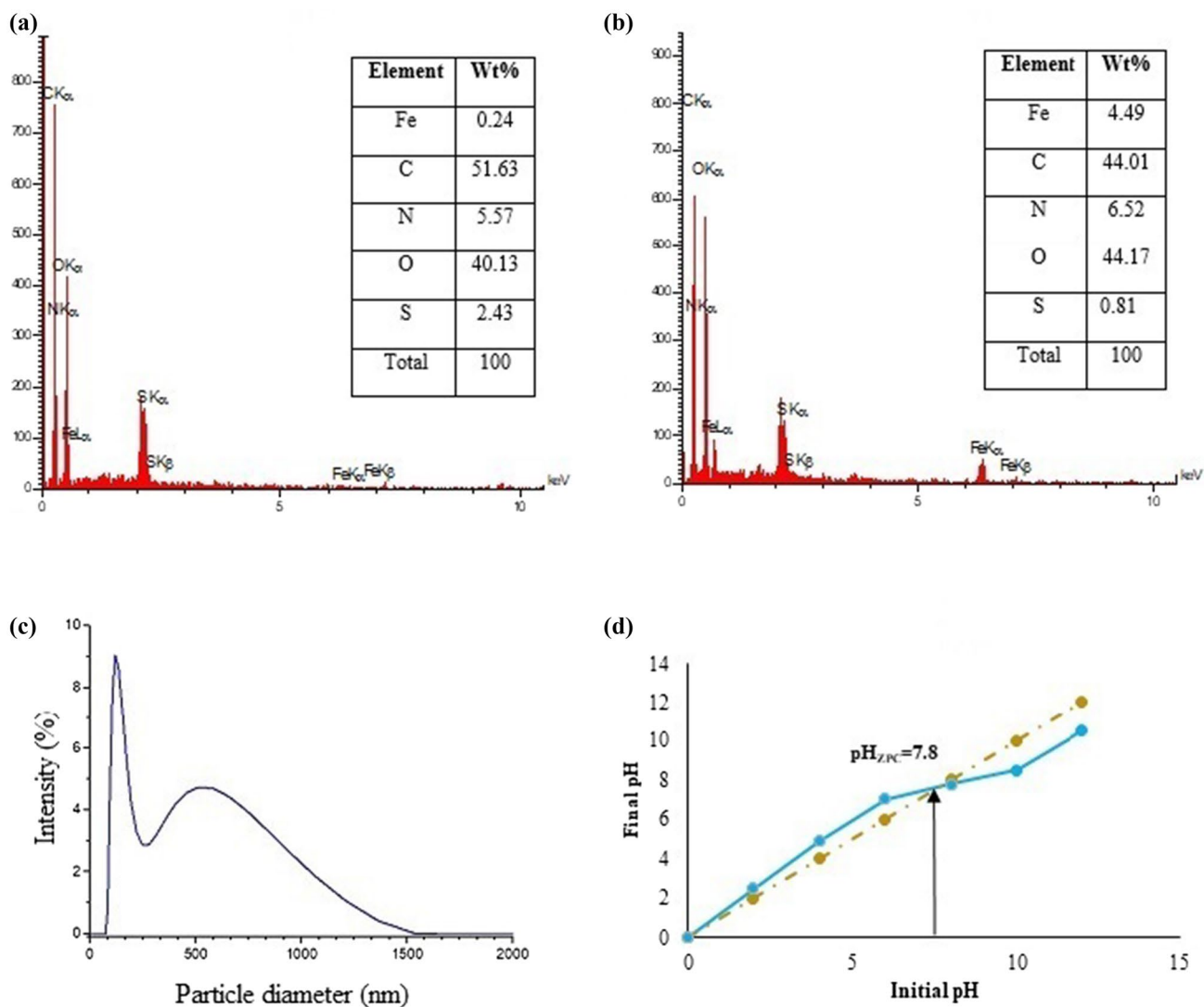


Fig. 4 EDX spectra and elemental composition of **a** SC, **b** Fe₃O₄/SC ncs, **c** DLS spectrum of synthesized Fe₃O₄/SC ncs, and **d** plot between final pH versus initial pH of nanocomposites

diameter of Fe₃O₄/SC ncs was found to be 221 nm (Fig. 4c). From Fig. 3d, the pH_{pzc} for Fe₃O₄/SC ncs was determined 7.8. This means that the adsorbent surface has a negative charge or a positive charge for pH values above or below 7.8, respectively.

Modeling of the MG removal rate

In this study, the impacts of the main factors, including the initial MG concentration, Fe₃O₄/SC ncs dose, reaction time, and pH on the MG removal rate were surveyed. The data of MG removal using Fe₃O₄/SC ncs are given in Table 2.

From Table 2, the maximum and minimum removal rates were 87.92 and 15.09, respectively. The impact of the independent factors, including the initial MG level, Fe₃O₄/SC ncs dose, reaction time, and pH, on the MG removal

efficiency was assessed. Table 3 shows the statistical adequacy evaluation of models. The experimental findings were statistically evaluated for linear, 2FI, quadratic and cubic models to choose the model that best explains the data.

Based on the data in Table 3, the quadratic model was proposed to fit the experimental data. Table 4 offers comparative model regression findings. Table 4 estimates the coefficients for the quadratic model of MG removal by Fe₃O₄/SC.

From Table 4, based on the coefficient values of each of the coded factors, the quadratic model for the removal efficiency (Y) can be expressed as the following equation:

$$Y = 58.09 + 8.95A - 9.59B + 23.15C + 7.59D + 4.01AB - 5.88AC - 2.06AD + 1.81BC + 4.08BD - 6.79CD + 3.84A^2 + 1.40B^2 - 1.41C^2 - 9.17D^2 \tag{4}$$

Table 2 BBD matrix for MG removal by Fe₃O₄/SC ncs

| Run no | Coded variable | | | | Removal (%) | Run no | Coded variable | | | | Removal (%) |
|--------|----------------|----|----|----|-------------|--------|----------------|----|----|----|-------------|
| | A | B | C | D | | | A | B | C | D | |
| 1 | -1 | 0 | 1 | 0 | 86.95 | 16 | 0 | 0 | 1 | -1 | 70.00 |
| 2 | 1 | -1 | 0 | 0 | 51.99 | 17 | -1 | -1 | 0 | 0 | 87.92 |
| 3 | 1 | 0 | 0 | -1 | 69.78 | 18 | 1 | 0 | 1 | 0 | 55.12 |
| 4 | 0 | 0 | 1 | 1 | 35.16 | 19 | 0 | -1 | 0 | -1 | 67.03 |
| 5 | -1 | 1 | 0 | 0 | 50.12 | 20 | 1 | 0 | 0 | 1 | 45.11 |
| 6 | 0 | 1 | 0 | 1 | 17.55 | 21 | 0 | -1 | -1 | 0 | 65.02 |
| 7 | -1 | 0 | -1 | 0 | 40.79 | 22 | 0 | 0 | 0 | 0 | 52.61 |
| 8 | 0 | 0 | -1 | 1 | 27.64 | 23 | 0 | 0 | 0 | 0 | 50.21 |
| 9 | 0 | 1 | 0 | -1 | 83.00 | 24 | 0 | 0 | 0 | 0 | 61.02 |
| 10 | 0 | -1 | 1 | 0 | 58.31 | 25 | 0 | -1 | 0 | 1 | 15.09 |
| 11 | -1 | 0 | 0 | 1 | 75.24 | 26 | 0 | 0 | -1 | -1 | 45.32 |
| 12 | 0 | 1 | 1 | 0 | 57.38 | 27 | 1 | 0 | -1 | 0 | 68.13 |
| 13 | 0 | 0 | 0 | 0 | 34.86 | 28 | 1 | 1 | 0 | 0 | 30.16 |
| 14 | -1 | 0 | 0 | -1 | 66.06 | 29 | 0 | 1 | -1 | 0 | 70.08 |
| 15 | 0 | 0 | 0 | 0 | 86.95 | | | | | | |

Table 3 Statistical adequacy evaluation of models

| Source | Sequential <i>p</i> -value | Lack of Fit <i>p</i> -value | Adjusted <i>R</i> ² | Predicted <i>R</i> ² |
|------------------|----------------------------|-----------------------------|--------------------------------|---------------------------------|
| Linear | <0.0001 | 0.36 | 0.80 | 0.74 |
| 2FI | 0.43 | 0.35 | 0.80 | 0.63 |
| Quadratic | 0.01 | 0.69 | 0.89 | 0.77 |
| Cubic | 0.54 | 0.64 | 0.88 | 0.29 |

According to Eq. 4, each model consisted of both fixed and variable parts. Also, the removal efficiency was 85.98%, which is affected by various parameters. The coded factors of A, B, C, and D had the coefficients of +8.95, -9.59, +23.15, and +7.59, respectively. The pH (C code) with a coefficient of +23.15 had the highest impact on the MG removal. The greatest interaction is related to CD with a coefficient of -6.79, and the greatest square effect of factors is related to D² with a coefficient of -9.17.

Table 4 Coefficients of estimation for quadratic model of MG removal by Fe₃O₄/SC ncs

| Factor | Coefficient estimate | df | Standard error | 95% CI low | 95% CI high | VIF |
|----------------|----------------------|----|----------------|------------|-------------|------|
| Intercept | 58.09 | 1 | 2.92 | 51.82 | 64.36 | |
| A-Time | 8.95 | 1 | 1.89 | 4.90 | 12.99 | 1 |
| B-Conc | -9.59 | 1 | 1.89 | -13.64 | -5.55 | 1 |
| C-pH | 23.15 | 1 | 1.89 | 19.10 | 27.19 | 1 |
| D-Dose | 7.59 | 1 | 1.89 | 3.54 | 11.63 | 1 |
| AB | 4.01 | 1 | 3.27 | -2.99 | 11.02 | 1 |
| AC | -5.88 | 1 | 3.27 | -12.89 | 1.12 | 1 |
| AD | -2.06 | 1 | 3.27 | -9.06 | 4.95 | 1 |
| BC | 1.81 | 1 | 3.27 | -5.20 | 8.82 | 1 |
| BD | 4.08 | 1 | 3.27 | -2.92 | 11.09 | 1 |
| CD | -6.79 | 1 | 3.27 | -13.80 | 0.2175 | 1 |
| A ² | 3.84 | 1 | 2.57 | -1.67 | 9.34 | 1.08 |
| B ² | 1.40 | 1 | 2.57 | -4.11 | 6.90 | 1.08 |
| C ² | -1.41 | 1 | 2.57 | -6.91 | 4.10 | 1.08 |
| D ² | -9.17 | 1 | 2.57 | -14.67 | -3.67 | 1.08 |

Table 5 Analysis of variance (ANOVA) for quadratic model of MG removal by Fe₃O₄/SC ncs

| | Sum of squares | df | Mean square | F-value | p-value |
|-------------------------|----------------|----|--------------------------|---------|---------|
| Model | 10,461.89 | 14 | 747.28 | 17.50 | <0.0001 |
| A—Time | 960.34 | 1 | 960.34 | 22.49 | 0.0003 |
| B—Conc | 1103.81 | 1 | 1103.81 | 25.85 | 0.0002 |
| C—pH | 6428.76 | 1 | 6428.76 | 150.56 | <0.0001 |
| D—Dose | 690.84 | 1 | 690.84 | 16.18 | 0.0013 |
| AB | 64.40 | 1 | 64.40 | 1.51 | 0.2397 |
| AC | 138.42 | 1 | 138.42 | 3.24 | 0.0934 |
| AD | 16.93 | 1 | 16.93 | 0.3966 | 0.5390 |
| BC | 13.10 | 1 | 13.10 | 0.3069 | 0.5883 |
| BD | 66.75 | 1 | 66.75 | 1.56 | 0.2317 |
| CD | 184.42 | 1 | 184.42 | 4.32 | 0.0566 |
| A ² | 95.45 | 1 | 95.45 | 2.24 | 0.1571 |
| B ² | 12.64 | 1 | 12.64 | 0.2961 | 0.5949 |
| C ² | 12.83 | 1 | 12.83 | 0.3005 | 0.5922 |
| D ² | 545.32 | 1 | 545.32 | 12.77 | 0.0031 |
| Residual | 597.78 | 14 | 42.70 | | |
| Lack of Fit | 383.47 | 10 | 38.35 | 0.7157 | 0.6966 |
| Pure Error | 214.31 | 4 | 53.58 | | |
| Cor Total | 11,059.67 | 28 | | | |
| R ² | 0.94 | | Predicted R ² | 0.77 | |
| Adjusted R ² | 0.89 | | Adeq Precision | 16.81 | |

Fig. 5 Distribution of experimental vs. predicted removal for MG adsorption onto Fe₃O₄/SC ncs

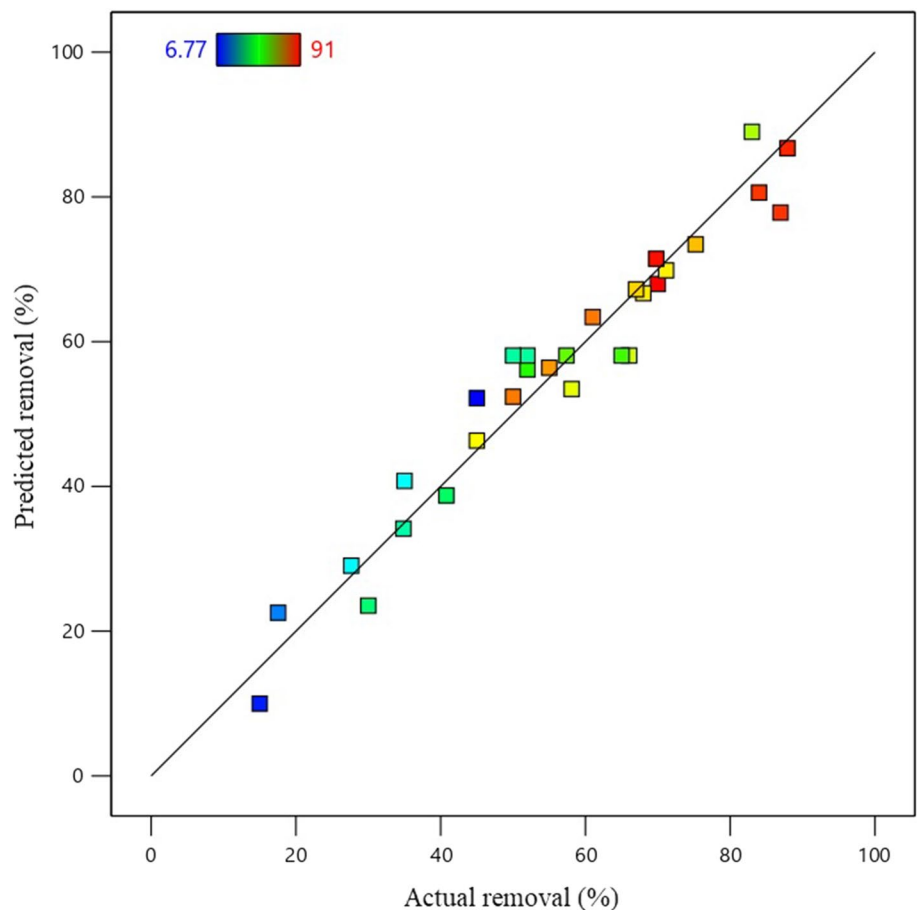


Table 5 presents ANOVA for the response surface quadratic model. Overall, the results of Table 5 showed that the model was significant (P -value < 0.05). Accordingly, the values of R^2 , adjusted R^2 , predicted R^2 , and adequacy precision were obtained 0.94, 0.89, 0.77, and 16.81, respectively.

For each of the main coded values in Table 5, the P -value was less than 0.05, indicating that the MG removal rate was statistically significant. It is recommended that the difference between the set R^2 and the predicted R^2 should be less than 0.2, which is true for the model.

The adequacy precision term measures the signal-to-noise ratio. This parameter was 16.81, which is higher than the minimum desired value of 4. Figure 5 displays the actual removal versus the predicted removal. As shown in Fig. 5, the adequacy of the model to provide a good prediction for MG removal is clear.

Main and interaction impacts

Figure 6a-b depicts the impact of contact time, MG concentration, pH, and Fe₃O₄/SC ncs dose on the MG removal rate.

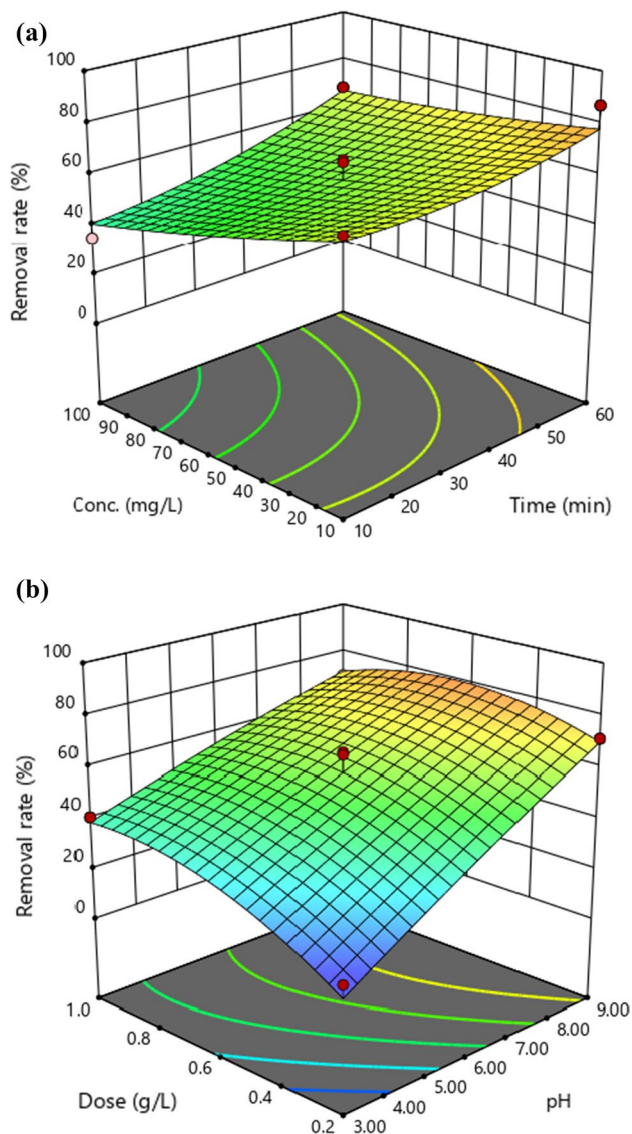


Fig. 6 Response surface plot about the effects of **a** Conc. vs. time, **b** dose vs. pH

Initial dye concentration and its effect

From Fig. 6a, increasing the dye concentration has an inverse effect on its removal efficiency (P -value < 0.05). The MG removal efficiency at concentrations of 10 and 100 mg/L was observed 68 and 47%, respectively, keeping the other experimental conditions constant. The decreasing trend of removal efficiency with increasing concentration can be due to the presence of large empty sites on the adsorbent surface to absorb dye at low dye concentrations, while the saturation of active binding sites with dye molecules at higher concentrations reduced the MG removal efficiency (Wu et al. 2016; Aliasghar Navaei et al. 2019).

Contact time and its effect

Figure 6a shows that with increasing time from 10 to 60 min, the removal efficiency increased by 25% (P -value < 0.05). The removal of malachite in the early times, due to the availability of a large number of free surface active sites to absorb the dye, is done more quickly and then gradually the slope of the dye removal process is slowed down. This indicates that over time, the active sites become saturated and their number decreases (Davodi et al. 2019; Kataria and Garg 2019).

The pH effect study

The pH is an effective factor on the ionization of the adsorbent and the surface charge, which had the greatest effect on the dye adsorption process. The findings of Fig. 6b show that with increasing the pH from 3 to 9, the dye removal also increased from 33.53 to 79.52%, respectively. The pH_{zpc} of Fe_3O_4/SC ncs was obtained 7.8. Thus, at pH below 7.8, the charge on the adsorbent surface becomes positive, leading to the reply of cationic dye molecule. At low pH, there is a high density between the positive ions of the MG cationic dye and the H^+ ions, which ultimately reduces the removal efficiency (Foroutan et al. 2020a). In other words, the adsorbent surface at a pH less than 7.8 is positively charged, which leads to the repulsion of dye molecules. At pH above 7.8, the negatively charged adsorbent surface absorbs the positively charged dye molecules and the number of H^+ ions decreases rapidly. This results in less competition between H^+ ions and cationic dye molecules adsorbed at active sites (Wu et al. 2016; Ali et al. 2017; Saini et al. 2017).

Adsorbent dose effect

From Fig. 6b, the removal MG efficiency is directly related to the increase in Fe_3O_4/SC ncs dose (P -value < 0.05). As can be deduced from Fig. 8, by enhancing Fe_3O_4/SC ncs dose from 0.2 to 1 g/L, the MG removal rate was enhanced from 41.3 to 56.5% and then decreased slightly. This is a normal behavior of most sorption processes. Based on the adsorption theory, the contaminants are attracted to the sorption sites on the adsorbent surface (Nasoudari et al. 2021). Our findings are in agreement with those reported previously for the adsorption of the dye onto bimetallic chitosan particle (Asgari et al. 2013).

Optimum operational conditions

In this study, the results were analyzed using the Box–Behnken model to obtain the highest dye removal rate. According to the quadratic model, the highest removal rate (89.22%) was found at the pH of 8.62, the contact time of

Table 6 The kinetic and isotherm parameters fitted for MG removal by Fe₃O₄/SC ncs

| Kinetic model | Linear form | Parameter | Value | | | | |
|-------------------------|--|-----------------------------------|-----------------------|-----------------------|-----------------------|------------------------|----------|
| | | | 25 mg L ⁻¹ | 50 mg L ⁻¹ | 75 mg L ⁻¹ | 100 mg L ⁻¹ | 120 mg L |
| Pseudo-first-order | $\text{Log}(q_e - q_t) = \log q_e - \frac{k_1}{2.303} \cdot t$ | $q_{e,\text{cal}}$ (mg/g) | 0.97 | 0.94 | 0.23 | 0.90 | 0.81 |
| | | K_1 (min ⁻¹) | 2.38 | 3.20 | 4.84 | 3.97 | 4.73 |
| | | R^2 | 0.85 | 0.83 | 0.92 | 0.95 | 0.91 |
| Pseudo-second-order | $\frac{t}{q_t} = \frac{1}{k_2 q_e^2} + \frac{1}{q_e} \cdot t$ | $q_{e,\text{cal}}$ (mg/g) | 12.22 | 5.232 | 61.72 | 42.37 | 27.62 |
| | | K_2 (min ⁻¹) | 0.002 | 0.001 | 0.0005 | 0.006 | 0.004 |
| | | R^2 | 0.91 | 0.86 | 0.95 | 0.99 | 0.99 |
| Intraparticle diffusion | $qt = k_p \cdot t^{0.5} + c$ | K_p (mg/g min ^{-0.5}) | 2.37 | 4.46 | 6.08 | 5.95 | 4.69 |
| | | R^2 | 0.95 | 0.99 | 0.87 | 0.93 | 0.77 |
| | | | | | | | |
| Isotherm model | Linear form | Parameter | Value | | | | |
| Langmuir | $\frac{C_e}{q_e} = \frac{1}{q_m} C_e + \frac{1}{q_m b}$ | q_{max} (mg/g) | 41.66 | | | | |
| | | K_L (L/mg) | 0.254 | | | | |
| | | R^2 | 0.973 | | | | |
| Freundlich | $\text{Log } q_e = \log K_F + \frac{1}{n} \log C_e$ | K_F mg/g(L/mg) ^{1/n} | 132.22 | | | | |
| | | n | 0.408 | | | | |
| | | R^2 | 0.967 | | | | |
| Temkin | $q_e = B_1 \ln k_t + B_1 \ln C_e$ | k_t (L/mg) | 20.07 | | | | |
| | | B_1 | 8.911 | | | | |
| | | R^2 | 0.914 | | | | |

59.86 min, the Fe₃O₄/SC ncs dose of 0.59 g /L and the MG level of 17.62 mg/L. Conduction of similar tests at specified optimum conditions reveals the high repeat ability of method for prediction of real removal percentage with relative deviation less than 2%.

Isotherm and kinetic models

The adsorption kinetics is one of the main parameters to simulate the solute adsorption rate from the solution–solution interface. This model provides useful information in the field of adsorption economics by evaluating the velocity constants and thus the contact time and volume of an adsorption unit (Mohebbad et al. 2019). The coefficients of reaction rate were calculated by the pseudo-first-order, pseudo-second-order and intraparticle diffusion kinetic models. Table 6 illustrates the parameters of kinetic and isotherm fitted for the MG removal using Fe₃O₄/SC ncs. From Table 6, R² for pseudo-first-order, pseudo-second-order, and intraparticle diffusion kinetics were 0.95, 0.99, and 0.93. The value of pseudo-second-order regression coefficient (R² = 0.99) is higher than that of other models. Hence, the pseudo-second-order model is best suited for

MG. In a study, adsorption data were more consistent with the pseudo-second-order kinetic model (Foroutan et al. 2020b). Also the equilibrium adsorption capacity value or Q_e (cal) is close to or almost equal to Q_e (experimental) value obtained from adsorption experiments of MG for the pseudo-second-order model.

In this study, experimental equilibrium information was evaluated using adsorption isotherm models including Langmuir, Freundlich, and Temkin models. The results of

Table 7 Comparison of Langmuir adsorption capacities of MG with results from previous studies

| Adsorbent | Adsorbate MG (mg g ⁻¹) | Reference |
|--|------------------------------------|-----------------------------|
| Fe ₃ O ₄ @ATPA@AMPA | 414.16 | (Melhi et al. 2022) |
| Alginate/Fe ₃ O ₄ | 48 | (Mohammadi et al. 2014) |
| Magnetic phosphate ncs | 90.9 | (Zhang et al. 2019) |
| SSW/Fe–Cu | 63.55 | (Blanco-Flores et al. 2020) |
| CoFe ₂ O ₄ @SiO ₂ | 75.5 | (Amiri et al. 2017) |
| Banana pseudo-stem fiber | 26.50 | (Neha et al. 2011) |
| Fe ₃ O ₄ /SC | 41.66 | Current study |

Table 6 show that the Langmuir model agrees with the equilibrium data (Wan et al. 2016). The Langmuir adsorption model is based on the assumption that maximum adsorption corresponds to a saturated monolayer of solute molecules on the adsorbent surface with no lateral interaction between the adsorbed molecules (Asgari et al. 2014). This indicates the monolayer adsorption of MG on $\text{Fe}_3\text{O}_4/\text{SC}$ ncs. According to Langmuir model, the maximum adsorption capacity of MG was obtained 41.66 mg/g. In the study of Foroutan et al. (2019), the maximum adsorption capacity of the ACSO/ Fe_3O_4 magnetic composite toward methylene blue reached as high as 60.60 mg/g, respectively (Foroutan et al. 2019). The adsorption capacities of MG with other reported adsorbents are listed in Table 7. These data propose that the $\text{Fe}_3\text{O}_4/\text{SC}$ ncs have potential to remove MG from aquatic environment.

Conclusion

In the current study, the biogenic green synthesis method was utilized to synthesize $\text{Fe}_3\text{O}_4/\text{SC}$ ncs. These nanocomposites were used for MG removal from aqueous environment. Process optimization was performed using the BBD. According to the quadratic model, the highest removal rate (89.22%) was found at the pH of 8.62, the contact time of 59.86 min, the $\text{Fe}_3\text{O}_4/\text{SC}$ ncs dose of 0.59 g/L, and the MG level of 17.62 mg/L. The MG removal rate follows the pseudo-second-order model and the Langmuir model. The maximum absorption capacity for MG was 41.66 mg/g. These findings suggest that the $\text{Fe}_3\text{O}_4/\text{SC}$ ncs has a significant potential for the MG adsorption of from aqueous solution.

Acknowledgements Not applicable.

Authors' contributions ZB wrote and edited the paper and conceived and designed the experiments; FK performed the experiments and wrote the paper; FA performed the experiments.

Funding The authors would like to thank the financial support provided by the Mashhad University of Medical Science (Iran) through the grant number of 980284.

Data availability All necessary data are included in the document.

Declarations

Conflict of interest The authors declare that they have no conflicts of interest.

Ethical approval This article does not contain any studies with human participants or animals performed by any of the authors.

Open Access This article is licensed under a Creative Commons Attribution 4.0 International License, which permits use, sharing,

adaptation, distribution and reproduction in any medium or format, as long as you give appropriate credit to the original author(s) and the source, provide a link to the Creative Commons licence, and indicate if changes were made. The images or other third party material in this article are included in the article's Creative Commons licence, unless indicated otherwise in a credit line to the material. If material is not included in the article's Creative Commons licence and your intended use is not permitted by statutory regulation or exceeds the permitted use, you will need to obtain permission directly from the copyright holder. To view a copy of this licence, visit <http://creativecommons.org/licenses/by/4.0/>.

References

- Ali AF, Kovo AS, Adetunji SA (2017) Methylene blue and brilliant green dyes removal from aqueous solution using agricultural wastes activated carbon. *JEAS* 7:95–107
- Aliasghar Navaei M, Alidadi H, Dankoob M, Bonyadi Z, Dehghan A, Hosseini A (2019) Biosorption of reactive red 120 dye from aqueous solution using *Saccharomyces cerevisiae*: RSM analysis, isotherms, and kinetic studies. *Desalin Water Treat* 171:418–427
- Amiri M, Salavati-Niasari M, Akbari A, Gholami T (2017) Removal of malachite green (a toxic dye) from water by cobalt ferrite silica magnetic nanocomposite: herbal and green sol-gel autocombustion synthesis. *Int J Hydrog Energy* 42:24846–24860
- Asgari G, Ramavandi B, Farjadfar S (2013) Abatement of azo dye from wastewater using bimetal-chitosan. *Sci World J* 476271:1–10
- Asgari G, Ramavandi B, Sahebi S (2014) Removal of a cationic dye from wastewater during purification by *Phoenix dactylifera*. *Desalin Water Treat* 52:7354–7365
- Bayat M, Beyki MH, Shemirani F (2015) One-step and biogenic synthesis of magnetic Fe_3O_4 -Fir sawdust composite: application for selective preconcentration and determination of gold ions. *J Ind Eng Chem* 21:912–919
- Blanco-Flores A, Toledo-Jaldin HP, Vilchis-Néstor AR, López-Téllez G, Sánchez-Mendieta V, Ávila-Márquez DM (2020) Metallurgical slag properties as a support material for bimetallic nanoparticles and their use in the removal of malachite green dye. *Adv Powder Technol* 31:2853–2865
- Bonyadi Z, Nasoudari E, Ameri M, Ghavami V, Shams M, Sillanpää M (2022) Biosorption of malachite green dye over *Spirulina platensis* mass: process modeling, factors optimization, kinetic, and isotherm studies. *Appl Water Sci* 12:1–11
- Chen J, Hao Y, Chen M (2014) Rapid and efficient removal of Ni^{2+} from aqueous solution by the one-pot synthesized EDTA-modified magnetic nanoparticles. *ESPR* 21:1671–1679
- Cheng Z, Gao Z, Ma W, Sun Q, Wang B, Wang X (2012) Preparation of magnetic Fe_3O_4 particles modified sawdust as the adsorbent to remove strontium ions. *Chem Eng J* 209:451–457
- Chowdhury MF, Khandaker S, Sarker F, Islam A, Rahman MT, Awual MR (2020) Current treatment technologies and mechanisms for removal of indigo carmine dyes from wastewater: a review. *J Mol Liq*, 114061.
- Davodi M, Alidadi H, Ramezani A, Jamali-Behnam F, Bonyadi Z (2019) Study of the removal efficiency of arsenic from aqueous solutions using *Melia azedarach* sawdust modified with FeO : isotherm and kinetic studies. *Desalin Water Treat* 137:292–299
- Esvandi Z, Foroutan R, Peighambari SJ, Akbari A, Ramavandi B (2020) Uptake of anionic and cationic dyes from water using natural clay and clay/starch/ MnFe_2O_4 magnetic nanocomposite. *Surf Interfaces* 21:100754
- Fan X, Deng L, Li K, Lu H, Wang R, Li W (2021) Adsorption of malachite green in aqueous solution using sugarcane bagasse-barium carbonate composite. *Colloids Interface Sci Commun* 44:100485

- Foroutan R, Mohammadi R, Razeghi J, Ramavandi B (2019) Performance of algal activated carbon/Fe₃O₄ magnetic composite for cationic dyes removal from aqueous solutions. *Algal Res* 40:101509
- Foroutan R, Mohammadi R, MousaKhanloo F, Sahebi S, Ramavandi B, Kumar PS, Vardhan KH (2020a) Performance of montmorillonite/graphene oxide/CoFe₂O₄ as a magnetic and recyclable nanocomposite for cleaning methyl violet dye-laden wastewater. *Adv Powder Technol* 31:3993–4004
- Foroutan R, Mohammadi R, Sohrabi N, Sahebi S, Farjadfar S, Esvandi Z, Ramavandi B (2020b) Calcined alluvium of agricultural streams as a recyclable and cleaning tool for cationic dye removal from aqueous media. *Environ Technol Innov* 17:100530
- Foroutan R, Peighambaroust SJ, Esvandi Z, Khatooni H, Ramavandi B (2021) Evaluation of two cationic dyes removal from aqueous environments using CNT/MgO/CuFe₂O₄ magnetic composite powder: A comparative study. *J Environ Chem Eng* 9:104752
- Gan W, Gao L, Zhan X, Li J (2016) Preparation of thiol-functionalized magnetic sawdust composites as an adsorbent to remove heavy metal ions. *RSC Adv* 6:37600–37609
- Joshi S, Garg V, Kataria N, Kadirvelu K (2019) Applications of Fe₃O₄@ AC nanoparticles for dye removal from simulated wastewater. *Chemosphere* 236:124280
- Joshi S, Garg V, Saini J, Kadirvelu K (2018) Removal of toulidine blue dye from aqueous solution by silica-iron oxide nanoparticles. *Mater Focus* 7:140–146
- Kataria N, Garg V (2018) Green synthesis of Fe₃O₄ nanoparticles loaded sawdust carbon for cadmium (II) removal from water: regeneration and mechanism. *Chemosphere* 208:818–828
- Kataria N, Garg V (2019) Application of EDTA modified Fe₃O₄/sawdust carbon nanocomposites to ameliorate methylene blue and brilliant green dye laden water. *Environ Res* 172:43–54
- Liu Y, Fu R, Sun Y, Zhou X, Baig SA, Xu X (2016) Multifunctional nanocomposites Fe₃O₄@ SiO₂-EDTA for Pb (II) and Cu (II) removal from aqueous solutions. *Appl Surf Sci* 369:267–276
- Melhi S, Algamdi M, Alqadami AA, Khan MA, Alosaimi EH (2022) Fabrication of magnetically recyclable nanocomposite as an effective adsorbent for the removal of malachite green from water. *Chem Eng Res Des* 177:843–854
- Mohammadi A, Daemi H, Barikani M (2014) Fast removal of malachite green dye using novel superparamagnetic sodium alginate-coated Fe₃O₄ nanoparticles. *Int J Biol Macromol* 69:447–455
- Mohebbad B, Bonyadi Z, Dehghan AA, Rahmat MH (2019) Arsenic removal from aqueous solutions using *Saccharomyces cerevisiae*: Kinetic and equilibrium study. *Environ Prog Sustain Energy* 38:S398–S402
- Nasoudari E, Ameri M, Shams M, Ghavami V, Bonyadi Z (2021) The biosorption of Alizarin Red S by *Spirulina platensis*; process modelling, optimisation, kinetic and isotherm studies. *J Environ Anal Chem*, pp 1–15.
- Neha G, Kushwaha AK, Chattopadhyaya M (2011) Kinetics and thermodynamics of malachite green adsorption on banana pseudo-stem fibers. *J Chem Pharm Res* 3:284–296
- Qu W, Yuan T, Yin G, Xu S, Zhang Q, Su H (2019) Effect of properties of activated carbon on malachite green adsorption. *Fuel* 249:45–53
- Ramavandi B, Farjadfar S, Ardjmand M (2014) Mitigation of orange II dye from simulated and actual wastewater using bimetallic chitosan particles: Continuous flow fixed-bed reactor. *J Environ Chem Eng* 2:1776–1784
- Ramavandi B, Najafpoor AA, Alidadi H, Bonyadi Z (2019) Alizarin red-S removal from aqueous solutions using *Saccharomyces cerevisiae*: kinetic and equilibrium study. *Desalin Water Treat* 144:286–291
- Saini J, Garg V, Gupta R, Kataria N (2017) Removal of Orange G and Rhodamine B dyes from aqueous system using hydrothermally synthesized zinc oxide loaded activated carbon (ZnO-AC). *J Environ* 5:884–892
- Selvaraj V, Karthika TS, Mansiya C, Alagar M (2021) An over review on recently developed techniques, mechanisms and intermediate involved in the advanced azo dye degradation for industrial applications. *J Mol Struct* 1224:129195
- Tkaczyk A, Mitrowska K, Posyniak A (2020) Synthetic organic dyes as contaminants of the aquatic environment and their implications for ecosystems: A review. *Sci Total Environ* 717:137222
- Wan S, Hua Z, Sun L, Bai X, Liang L (2016) Biosorption of nitroimidazole antibiotics onto chemically modified porous biochar prepared by experimental design: Kinetics, thermodynamics, and equilibrium analysis. *Proc Saf Environ Protect* 104:422–435
- Wang Y, Yang J, Shen Y, Sun Y, Xiao Z, Lei H, Wang H, Xu Z (2017) Novel haptens synthesis and development of a monoclonal antibody-based enzyme-linked immunosorbent assay for leuco-malachite green in fish. *Food Agric Immunol* 28:1460–1476
- Wu X-L, Shi Y, Zhong S, Lin H, Chen J-R (2016) Facile synthesis of Fe₃O₄-graphene@ mesoporous SiO₂ nanocomposites for efficient removal of Methylene Blue. *Appl Surf Sci* 378:80–86
- Yu X, Tong S, Ge M, Zuo J, Cao C, Song W (2013) One-step synthesis of magnetic composites of cellulose@ iron oxide nanoparticles for arsenic removal. *J Mater Chem A* 1:959–965
- Zhang F, Tang X, Huang Y, Keller AA, Lan J (2019) Competitive removal of Pb²⁺ and malachite green from water by magnetic phosphate nanocomposites. *Water Res* 150:442–451

Publisher's Note Springer Nature remains neutral with regard to jurisdictional claims in published maps and institutional affiliations.